Covalent Organic Frameworks

International Edition: DOI: 10.1002/anie.201913802
German Edition: DOI: 10.1002/ange.201913802

Combined Intrinsic and Extrinsic Proton Conduction in Robust Covalent Organic Frameworks for Hydrogen Fuel Cell Applications

*Yi Yang, Xueyi He, Penghui Zhang, Yassin H. Andaloussi, Hailu Zhang, Zhongyi Jiang, Yao Chen, Shengqian Ma, Peng Cheng, and Zhenjie Zhang**

Dedicated to the 100th anniversary of Nankai University

Abstract: *Developing new materials for the fabrication of proton exchange membranes (PEMs) for fuel cells is of great significance. Herein, a series of highly crystalline, porous, and stable new covalent organic frameworks (COFs) have been developed by a stepwise synthesis strategy. The synthesized COFs exhibit high hydrophilicity and excellent stability in strong acid or base (e.g., 12 M NaOH or HCl) and boiling water. These features make them ideal platforms for proton conduction applications. Upon loading with H_3PO_4, the COFs (H_3PO_4@COFs) realize an ultrahigh proton conductivity of 1.13×10^{-1} S cm^{-1}, the highest among all COF materials, and maintain high proton conductivity across a wide relative humidity (40–100 %) and temperature range (20–80 °C). Furthermore, membrane electrode assemblies were fabricated using H_3PO_4@COFs as the solid electrolyte membrane for proton exchange resulting in a maximum power density of 81 mW cm^{-2} and a maximum current density of 456 mA cm^{-2}, which exceeds all previously reported COF materials.*

Introduction

Global energy demand is continuously increasing, but energy supply is still mostly derived from the combustion of fossil fuels, which unavoidably brings about severe environment issues, such as air and water pollution.[1] Thus, developing clean and renewable energy is in urgent demand. Hydrogen fuel is an ideal candidate to address this challenge due to its high energy density and clean combustion product (i.e., water).[2–4] Hydrogen fuel cell (HFC) technology, especially proton exchange membrane (PEM) fuel cells, offer a clean and reliable alternative energy source due to their high energy conversion efficiency, zero emissions, and mild operating conditions.[5] Currently, exploring new proton conducting materials that can serve as solid electrolyte membranes of PEM fuel cells is a primary focus in this field.[6–11] At present, few materials offer the high proton conductivity and long working life necessary for commercial application, with the main exception being Nafion, a perfluorinated sulfonated polymer. However, the high cost, synthetic challenges and restricted operating conditions hinders further application.[12,13] Therefore, developing alternative materials to fabricate PEMs is of great significance and urgently needed.

Organic polymers have offered great promise for PEMs owing to their potential for high porosity, good structure robustness, and facile membrane fabrication.[14–20] However, traditional organic polymers are amorphous and well-defined control of structure and pore environments (i.e. pore size, shape and exposed functional groups) is difficult to achieve, thereby leading to a lack of thorough understanding of the structure–property relationships involved.[21,22] In the past decade, covalent organic frameworks (COFs) have emerged as a new class of crystalline porous organic polymer materials and demonstrated great potential to overcome the limits of conventional organic polymers owing to their well-defined structures, high surface areas, fine-tunable pore environments, and custom-design functionalities.[23–35] These advantages render COFs a promising platform for proton conductivity and PEMs. Recently, significant progress has been made by Dichtel,[36] Banerjee,[37] our group,[38] and others[39] to fabricate high-performance COF membranes. The Banerjee group achieved a benchmark proton conductivity (7.8×10^{-2} S cm^{-1}) for a freestanding COF membrane that further

[*] Y. Yang, P. Zhang, Prof. P. Cheng, Prof. Z. Zhang
Renewable energy conversion and storage center, College of Chemistry, Nankai University
Tianjin 300071 (China)
E-mail: zhangzhenjie@nankai.edu.cn
Prof. Y. Chen, Prof. Z. Zhang
State Key Laboratory of Medicinal Chemical biology, Nankai University
Tianjin 300071 (China)
X. He, Prof. Z. Jiang
School of Chemical Engineering and Technology, Tianjin University
Tianjin 300072 (China)
Prof. P. Cheng, Prof. Z. Zhang
Key Laboratory of Advanced Energy Materials Chemistry, Ministry of Education, Nankai University
Tianjin 300071 (China)
Y. H. Andaloussi
Department of Chemical Sciences, Bernal Institute, University of Limerick
Limerick V94 T9PX (Republic of Ireland)
Prof. H. Zhang
Suzhou institute of Nano-Tech and Nano-Bionics, Chinese Academy of Sciences
Suzhou 215123 (China)
Prof. S. Ma
Department of Chemistry, University of South Florida
4202 East Fowler Avenue, Tampa, FL 33620 (USA)
Supporting information and the ORCID identification number(s) for the author(s) of this article can be found under: https://doi.org/10.1002/anie.201913802.

served as the PEM of a membrane electrode assembly (MEA) and delivered the highest power output (maximum 24 mW cm^{-2}) among all reported COFs.[40] Currently, there are two facile strategies to fabricate proton conductive COF materials: 1) Fabricating intrinsic proton conductive COFs through the covalent incorporation of proton donor groups such as sulfonate, imidazole, and phenolic hydroxy groups into COF skeletons;[41] 2) endowing COFs with extrinsic proton conductivity through doping of proton carriers such as H_3PO_4 into COF pores.[42–46] For this strategy, COFs should possess functional groups with high binding affinity to the proton carriers to prevent leakage. For example, azo (N=N) groups can bind with $H_2PO_4^-$ anion from H_3PO_4 through hydrogen bonds to facilitate proton conduction.[42,47] To maximize the conductivity performance of COFs, a feasible approach is to combine the above two strategies to fabricate COFs with both intrinsic and extrinsic proton conductivity in one system.

In this study, we created a stepwise synthesis strategy to create COFs with multiple bond linkages and functional groups that are not easily produced by the traditional one-step synthesis strategy (Scheme 1). A series of highly porous and robust COFs (**NKCOF-1**, **-2**, **-3**, **-4**, NKCOF = Nankai Covalent Organic Framework) with an abundance of proton-accepting and donating groups were successfully synthesized through this stepwise synthesis strategy. The resultant NKCOFs possess azo groups that allow the doping of H_3PO_4, for extrinsic proton conductivity, while phenolic hydroxy groups present in NKCOFs serve as acids to directly donate protons for intrinsic proton conductivity. Meanwhile, the azo groups and phenolic hydroxy groups endow NKCOFs with high hydrophilicity, which promotes the absorption of water molecules into COF pores and thereby facilitates the proton conducting process.

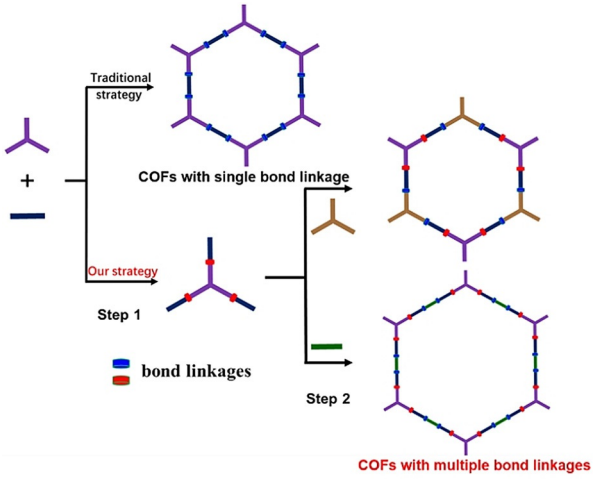

Scheme 1. Illustration of traditional one-step synthesis strategy of COFs with single bond linkage and our synthesis strategy to fabricate multifunctional COFs with multiple bond linkages.

Results and Discussion

To demonstrate the strategy to design proton conductive COFs, a series of NKCOFs with an abundance of azo and phenolic hydroxy groups were synthesized (Figure 1 a). Taking **NKCOF-1** as a representative example to explain the synthesis process, a C_3-symmetric precursor of **Azo-NHBoc** with three azo groups and three phenolic hydroxyl groups was first synthesized from a reaction of *N*-Boc-*p*-phenylenediamine with phloroglucinol under mild conditions (yield ≈ 80 %) (Supporting Information, Figures S1–S3). Subsequently, **Azo-NHBoc** monomer was reacted with 1,3,5-triformylphloroglucinol (TP) in a mixed solvent of mesity-

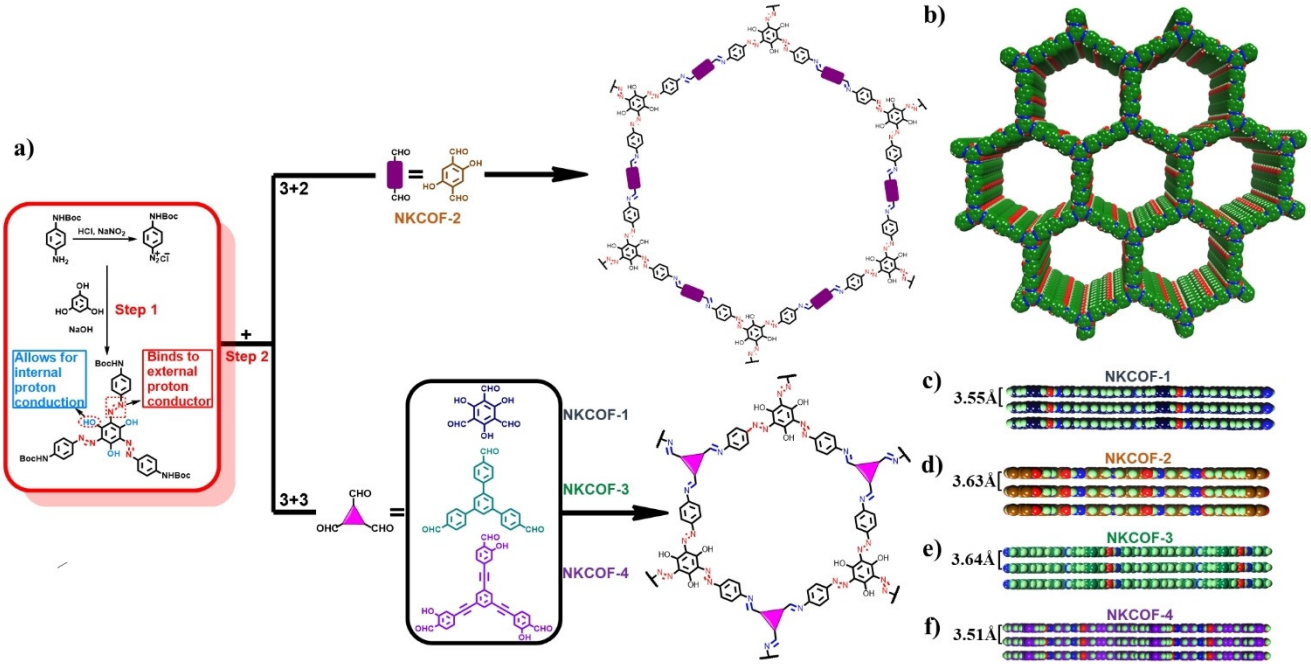

Figure 1. a) Illustration of the synthetic route of NKCOFs. b) The hexagonal structural of NKCOFs. c–f) The side views of **NKCOF-1**, **-2**, **-3**, and **-4**, respectively, resulting from the eclipsed AA stacking.

lene, 1,4-dioxane, 6 M acetic acid, and trifluoroacetic acid for 3 days at 120 °C. A black powder of **NKCOF-1** was harvested in a yield of 85 %. Adopting identical synthetic procedures and replacing TP with other aldehydes such as 2,5-dihydroxyterephthalaldehyde (DPA), 1,3,5-tri(4-formylphenyl)benzene (TFB), and 1,3,5-tri(3-hydroxy-4-formyl-ethynylphenyl)benzene (THEB) (Figure S4–S6) afforded **NKCOF-2**, **-3**, and **-4** (yield: 84 %, 90 %, and 87 %), respectively (Figure S7). It is notable that this is a rare example of directly reacting -NHBOC with -CHO groups to synthesize new COFs. This synthetic method was verified by synthesis of a model compound by reaction of **Azo-NHBoc** with 2-hydroxybenzaldehyde (Figure S8–S10).

Attributed to this stepwise synthesis strategy, various bond linkages and functional groups can be introduced into the skeleton of afforded COFs, which may otherwise be difficult to produce. The formation of NKCOFs were confirmed by FTIR spectroscopy and solid-state ^{13}C cross-polarization magic angle spinning nuclear magnetic resonance (CP-MAS NMR). Compared with the corresponding aldehydes and **Azo-NHBoc** monomer, FTIR spectra of the NKCOFs showed the disappearance of characteristic absorption peaks of aldehyde C=O (1634–1682 cm^{-1}) stretching bands, and the disappearance of N–H (3306 cm^{-1}), C=O (1704 cm^{-1}) and C–H (2978 cm^{-1}, 2931 cm^{-1}) stretching bands from **Azo-NHBoc** (Figure 2a and Figure S11). The

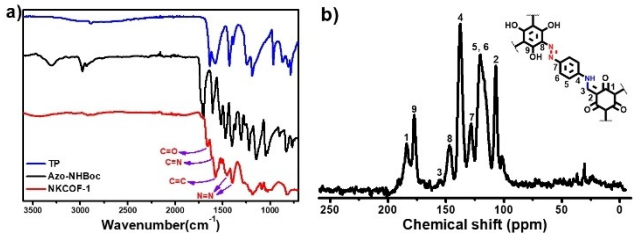

Figure 2. a) FTIR spectra of **NKCOF-1** compared with reactants. b) ^{13}C CP-MAS NMR spectra of **NKCOF-1**.

appearance of characteristic signals for the two distinct bond linkages of C=N (stretching bands at 1614–1687 cm^{-1}) and N=N (stretching bands at 1453–1473 cm^{-1}, and 1397–1402 cm^{-1}) finally confirmed the successful construction of the NKCOFs. In addition, **NKCOF-1** showed peaks at 1575 cm^{-1} and 1660 cm^{-1} assigned to the stretching bands of C=C and C=O of the enol-keto tautomer form, respectively. **NKCOF-4** showed a peak at 2158 cm^{-1} assigned to stretching bands of the C≡C triple bond. The ^{13}C CP-MAS NMR spectra further confirmed the formation of COFs (Figure 2b and Figure S12). All NKCOFs possess a peak between 145–165 ppm assigned to the carbon of the imine bonds. Additionally, keto–enol tautomerism was observed in **NKCOF-1** with the peaks at 184 ppm assigned to the C=O (keto form), and 147 ppm, 102 ppm assigned to the C=C (enol form). **NKCOF-4** showed a characteristic peak at 91 ppm assigned to the C≡C triple bond.

The crystalline and porous structure of NKCOFs were verified by powder X-ray diffraction (PXRD) analysis, electron microscopy images, and nitrogen adsorption–desorption isotherms. As shown in Figure 3a, the PXRD pattern of **NKCOF-1** exhibits a major peak at 4.56° with minor peaks at 8.34° and 27.34°, assigned to 100, 110, and 001 faces, respectively. The observed PXRD pattern of **NKCOF-2** exhibited an intense peak at 2.32° along with peaks at 3.98°, 4.80°, 6.26°, 14.86°, and 27.22° which were assigned to the 100,

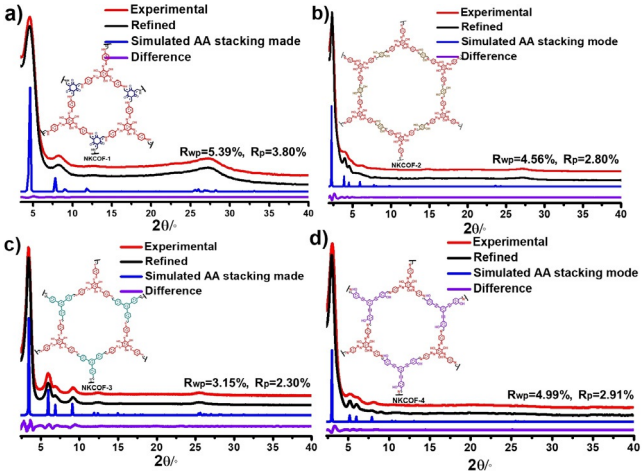

Figure 3. a) PXRD patterns of **NKCOF-1** and its structure. b) PXRD patterns of **NKCOF-2** and its structure. c) PXRD patterns of **NKCOF-3** and its structure. d) PXRD patterns of **NKCOF-4** and its structure.

110, 200, 210, 220, and 001 reflections (Figure 3b). **NKCOF-3** showed a very intense peak at 3.37° and five peaks at 5.95°, 6.83°, 9.15°, 12.41°, and 25.43° corresponding to the 100, 110, 200, 210, 220, and 001 reflections, respectively (Figure 3c). **NKCOF-4** showed five peaks at 3.14°, 5.46°, 6.30°, 8.34° and 27.04°, which were assigned to the 100, 110, 200, 210, and 001 reflections (Figure 3d). All experimental PXRD patterns of NKCOFs reflected good crystallinity and were consistent with the simulated patterns acquired from structural simulations according to an AA eclipsed layer stacking. Scanning electron microscopy (SEM) images revealed that **NKCOF-1** exhibited a distinctive morphology like nanowires about 200 nm in diameter (Figure 4a). The morphology of **NKCOF-2**, **-3**, and **-4** presented as micrometer-sized spheres comprised of nanometer-sized crystalline grains (Figure 4b and S13). The high-resolution transmission electron microscopy (HR-TEM) of NKCOFs showed distinct lattice fringes (Figure 4c–f and S14), indicative of the high crystallinity and two-dimensional layer structures of NKCOFs.

The permanent porosity of as-synthesized NKCOFs were assessed by N_2 adsorption isotherms collected at 77 K. As shown in Figure 5a, all NKCOFs showed rapid N_2 uptake at a comparatively low pressure range ($P/P_0 < 0.05$). **NKCOF-1** exhibited the type-I isotherm, indicative of its microporous nature. The sharp increase of adsorption for **NKCOF-1** under high pressure indicated the existence of macroporosity, likely generated by particle packing.[48] All other NKCOFs exhibited the typical type-IV isotherms, indicative of their mesoporous structures. The Langmuir specific surface areas were calculated to be 1011 $m^2 g^{-1}$, 1510 $m^2 g^{-1}$, 1139 $m^2 g^{-1}$ and 2612 $m^2 g^{-1}$ for **NKCOF-1**, **-2**, **-3**, **-4**, respectively (Figure S15–

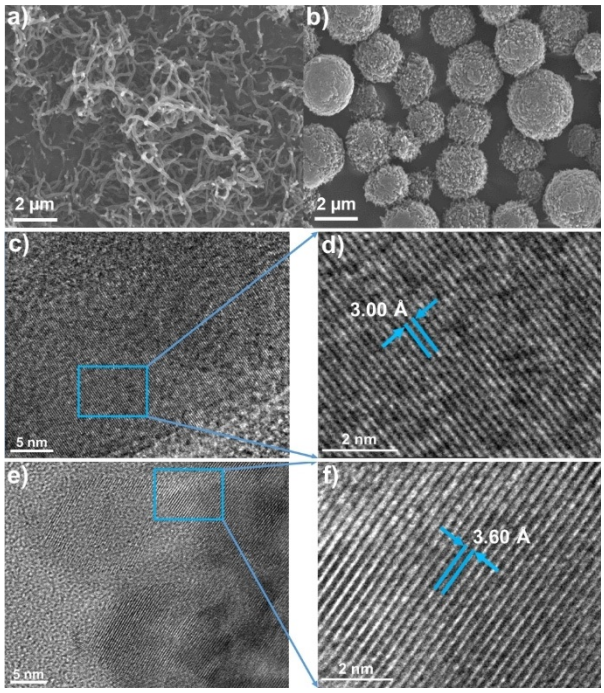

Figure 4. a) SEM image of **NKCOF-1**. b) SEM image of **NKCOF-2**. c) HR-TEM image of **NKCOF-1**. d) Partial enlarged detail of (c). e) HR-TEM image of **NKCOF-2**. f) Partial enlarged detail of (e).

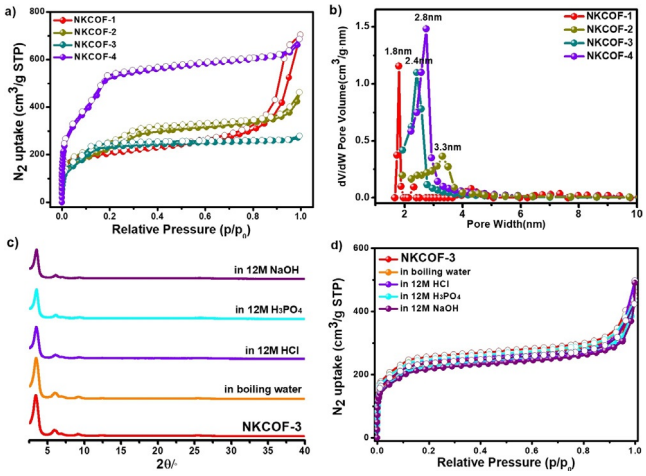

Figure 5. a) N_2 adsorption (solid symbols) and desorption (open symbols) isotherms of NKCOFs at 77 K. b) Pore size distribution of NKCOFs. c) PXRD patterns of pristine **NKCOF-3** (red) and after treatment for 2 days in boiling water (orange), 12 M HCl (violet), 12 M H_3PO_4 (cyan), and 12 M NaOH (purple). d) N_2 adsorption (solid symbols) and desorption (open symbols) isotherms of **NKCOF-3** (red) and after treatment for 2 days in boiling water (orange), 12 M HCl (violet), 12 M H_3PO_4 (cyan), and 12 M NaOH (purple).

S18). Pore size distribution calculated using density functional theory (DFT) revealed that **NKCOF-1**, **-2**, **-3**, **-4** possessed pore widths of 1.8, 3.3, 2.4, and 2.8 nm, respectively, which are in good agreement with the pore size established from the structural analysis and simulations (Figure 5b). The high surface areas and highly ordered nanopores make NKCOFs excellent platforms for loading and transferring substances.

Thermogravimetric analysis (TGA) was performed to determine thermal stability and confirm the absence of guest molecules inside the pores. The TGA curves of activated NKCOFs revealed that these COFs are thermal stability up to around 260 °C (Figure S19). The chemical stability of NKCOFs was examined by exposing NKCOFs to various harsh conditions. It was found that NKCOFs demonstrated excellent stability in acid, base, boiling water, and various organic solvents. Notably, **NKCOF-1**, **-3**, and **-4** were stable in concentrated HCl (12 M), concentrated H_3PO_4 (12 M) and concentrated NaOH (12 M) as verified by PXRD and N_2 sorption data (Figure 5c,d and Figures S20–S23). The high structure robustness and chemical stability of NKCOFs provide a powerful guarantee for their practical application.

NKCOFs possess a high density of azo and phenolic hydroxy groups. These functional groups make NKCOFs intrinsic proton conductive materials. Electrochemical impedance spectroscopy (EIS) was applied to measure the proton conductivities of NKCOFs in both hydrous and anhydrous conditions. NKCOFs were pressed into thin pellets, which exhibited good mechanical stability without breaking or fragmentation during testing. In anhydrous condition, the Nyquist plots of NKCOFs at 293 K and 353 K showed relatively low proton conductivity (Figure S24). However, once in hydrous condition, a dramatic increase of proton conductivity was observed. The proton conductivity was measured as 7.08×10^{-3} S cm^{-1}, 3.09×10^{-3} S cm^{-1}, 1.20×10^{-4} S cm^{-1}, and 5.43×10^{-3} S cm^{-1} for **NKCOF-1**, **-2**, **-3**, **-4**, respectively, at 353 K under 98% RH (Figure 6a, Figure S25 and Table S1). This water promotion phenomenon is consistent with the literature, which states that water molecules play a crucial role in the proton conduction process.[42,45,49,50] Moreover, phenolic hydroxy groups in NKCOFs are able to provide protons in the proton conduction process. In order to verify the contribution of the phenolic hydroxy groups to proton conductivity, **TpPa-1**,[51] an analogue of **NKCOF-1**,

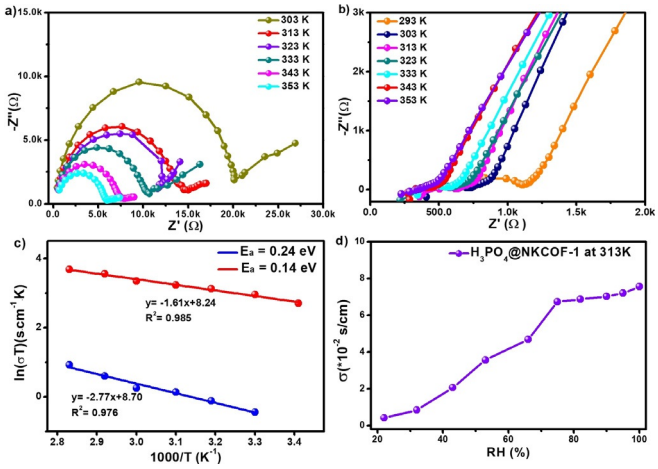

Figure 6. a) Nyquist plots of **NKCOF-1** measured under 98% RH at different temperatures. b) Nyquist plots of **H_3PO_4@NKCOF-1** measured under 98% RH at different temperatures. c) Arrhenius plots for **NKCOF-1** (blue) and **H_3PO_4@NKCOF-1** (red). d) Proton conductivity of **H_3PO_4@NKCOF-1** measured at 313 K under different relative humidity.

was selected as comparison (Figure S26). **TpPa-1** was synthesized through a reported Schiff base reaction between TP and *p*-phenylenediamine (PA) using solvothermal synthesis. Due to the keto–enol tautomerism, phenolic hydroxy groups mostly exist as the keto form in **TpPa-1**. As such, **TpPa-1** possesses fewer phenolic hydroxy groups than NKCOFs. As a result, the proton conductivity of **TpPa-1** (9.10×10^{-5} S cm^{-1}) was much lower than NKCOFs at 353 K under 98% RH (Figure S27 and Table S1) and as much as two orders of magnitude lower than the analogous **NKCOF-1**. These results highlight the increased proton conduction of NKCOFs due to intrinsic conductivity.

As reported in literature, azo groups exhibit a binding affinity to proton carriers such as H_3PO_4.[42,47] Thus, in order to further improve the proton conductivity of NKCOFs, a feasible approach is to incorporate H_3PO_4 as proton carriers due to its high proton content, low volatility (> 158 °C), high mobility, and conductivity.[52] After simply immersing NKCOFs into 5 M H_3PO_4 for 12 h and then washing thoroughly with water until the eluent reaches pH 7, the final loading of phosphoric acid calculated by TGA were 8.1 wt%, 2.0 wt%, 4.7 wt%, and 4.0 wt% for **H$_3$PO4@NKCOF-1**, **-2**, **-3**, **-4**, respectively (Figure S28–S31). Energy Dispersive X-Ray (EDX) spectroscopy mapping experiment further confirmed the existence of H_3PO_4 in COFs as indicated by the existence of well-dispersed P (Figures S32–S35). PXRD data revealed that NKCOFs loaded with H_3PO_4 (H_3PO_4@NKCOFs) retained their crystallinity (Figure S36) attributed to the high acid resistance of NKCOFs. N_2 sorption data revealed that H_3PO_4@NKCOFs showed reduced surface areas, due to the successful incorporation of H_3PO_4 into the pores of NKCOFs (Figures S37–S40). Additionally, SEM images showed that H_3PO_4@NKCOFs retained the particle morphology as the pristine NKCOFs (Figure S41).

EIS results revealed that the proton conductivity of H_3PO_4@NKCOFs were negligible under anhydrous conditions (Figure S42). However, values up to 4.69×10^{-2} S cm^{-1}, 1.12×10^{-2} S cm^{-1}, 2.06×10^{-4} S cm^{-1}, and 5.47×10^{-2} S cm^{-1} were measured for **H$_3$PO$_4$@NKCOF-1**, **-2**, **-3**, **-4**, respectively, at 293 K under 98% RH. When increasing the testing temperature, we found that the proton conductivity of H_3PO_4@NKCOFs increased (Figure 6b, Figures S43–S45 and Table S2) up to 1.13×10^{-1} S cm^{-1}, 4.28×10^{-2} S cm^{-1}, 1.12×10^{-2} S cm^{-1}, and 7.71×10^{-2} S cm^{-1} at 353 K under 98% RH. Notably, **H$_3$PO$_4$@NKCOF-1** sets up a new record (1.13×10^{-1} S cm^{-1}) for all reported COF materials, which exceeds the current record (7.8×10^{-2} S cm^{-1} for **PTSA@TpAzo** at 353 K under 95% RH)[40] and even comparable to the commercial Nafion (ca. 1×10^{-1} S cm^{-1} at 353 K under 98% RH)[12,53] (Table S3). In addition, when keeping **H$_3$PO$_4$@NKCOF-1** under continuous assessment for two days at 323 K under 98% RH, proton conductivity showed no reduction, implying no leakage of H_3PO_4 and high stability. Pellet stability was further demonstrated by soaking in water for 24 h which showed no evidence of the powder dispersing (Figure S46). Furthermore, TGA data revealed that the loading of phosphoric acid was maintained before and after EIS measurements (Figure S47), further indicating the strong binding of phosphoric acid in NKCOFs. The stability of all COF materials after EIS measurements was verified by the PXRD and N_2 sorption data, indicative of their intact structures (Figures S48–S51).

In order to investigate the proton conduction mechanism, **NKCOF-1** and **H$_3$PO$_4$@NKCOF-1** were examined further. There are two main mechanisms known for proton transport: the Grotthuss and the vehicular mechanisms, which can be identified primarily by activation energy (vehicular mechanisms > 0.4 eV; Grotthuss mechanisms < 0.4 eV).[22,50] As shown in Figure 5c, the activation energy (E_a) of **NKCOF-1** and **H$_3$PO$_4$@NKCOF-1** calculated by Arrhenius plots were 0.24 eV and 0.14 eV, respectively (Figure 6c). Thus, both **NKCOF-1** and **H$_3$PO$_4$@NKCOF-1** undergo the Grotthuss mechanism with protons "hopping" along the hydrogen bond network. The activation energy for **H$_3$PO$_4$@NKCOF-2**, **-3** and **-4** were calculated to be 0.24 eV, 0.40 eV and 0.08 eV, respectively, corresponding to Grotthuss transport mechanism. The activation energies of **H$_3$PO$_4$@NKCOF-1** and **-4** are notable for being lower than that of Nafion (0.22 eV).[54] In addition, we found that upon increasing the relative humidity, the proton conductivity of **H$_3$PO$_4$@NKCOF-1** increased (Figure 6d and Figure S52–S53), indicative of the crucial role of water in the conductive process. To explore the in-depth reason, hydrophobic angle measurements (Figure S54) and water vapor adsorption (Figure S55) were tested and revealed high hydrophilicity for both NKCOFs and H_3PO_4@NKCOFs. Thus, water molecule could form infinite networks of hydrogen bonds with functional groups and additives (e.g. azo, phenolic hydroxy and H_3PO_4) in H_3PO_4@NKCOFs to provide a highway for proton hopping transfer.

Encouraged by the high proton conductivity of H_3PO_4@NKCOFs, we further investigated their performances as solid electrolyte membranes for PEM fuel cell under H_2/O_2 operating conditions. Thin pellets were made of H_3PO_4@NKCOFs for use as the electrolyte membranes. Carbon papers coated with 60 wt% Pt/C catalyst were used as the anode and the cathode electrodes, and the Pt loading was kept as 0.5 mg cm^{-1} on each electrode. All of above were assembled into membrane electrode assemblies (MEAs) (Figure S56). Operating temperature was set at 60 °C and the flow rate of humid H_2 and O_2 were both 50 mL min^{-1}. The afforded MEAs exhibited open circuit voltages (OCVs) of 0.978 V, 0.953 V, 0.928 V, and 0.906 V for **H$_3$PO$_4$@NKCOF-1**, **-2**, **-3**, **-4**, respectively. The high OCV of MEAs indicated high proton conductivity of H_3PO_4@NKCOFs and good mechanical properties of the pellets without H_2 crossover. Moreover, the OCV maintained stability during the testing period (> 4 h) (Figure 7b and S57). As shown in Figure 7c (polarization curves), **H$_3$PO$_4$@NKCOF-1** membrane achieved a maximum power density of 81 mW cm^{-2}, much higher than other reported crystalline porous organic framework materials, and a maximum current density of 456 mA cm^{-2}. **H$_3$PO$_4$@NKCOF-2**, **-3**, and **-4** possessed maximum power density of 45 mW cm^{-2}, 24 mW cm^{-2}, and 56 mW cm^{-2}, respectively, and had maximum current density of 231 mA cm^{-2}, 133 mA cm^{-2}, and 269 mA cm^{-2} (Figure S58, Table S4). The maximum power density and the maximum current density were seen to positively correlate with materials' proton

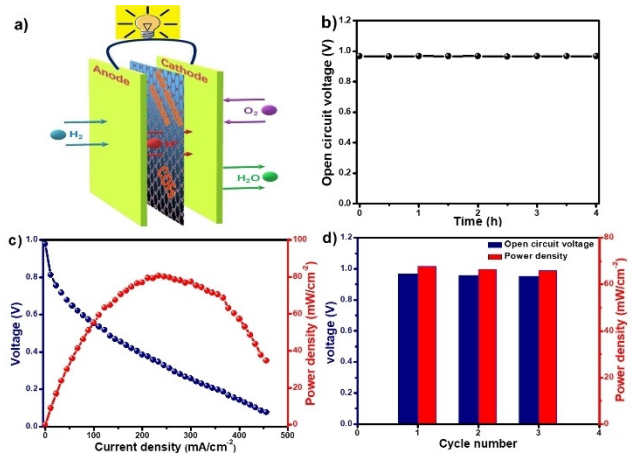

Figure 7. a) Scheme of the PEM fuel cells using H_3PO_4@NKCOFs as solid electrolyte membranes of MEA. b) Lifetime for OCV of **H_3PO_4@NKCOF-1**. c) Fuel cell polarization curves (navy) and power density curves (red) of **H_3PO_4@NKCOF-1** measured at 60 °C using single H_2/O_2 cell assembly under 100% RH. d) Cyclic stability of OCV (navy) and power density (red) of **H_3PO_4@NKCOF-1**.

conductivity. The cycle stability of the MEAs with H_3PO_4@NKCOFs membranes were examined, displaying that the OCV and the maximum power density remained stable for three cycles (Figure 7d). While powder-compressed pellets were successful in forming a PEM membrane that prevented fuel crossover, industrial applications would benefit from a self-standing membrane that may be continuously produced. Therefore, we fabricated large-sized, self-standing, flexible COF membranes (**NKCOF-1-M**, **-2-M**, **-3-M**, **-4-M**) (Figures S59–S60) through a method reported by the Banerjee's group.[40] H_3PO_4 was loaded into the NKCOF-Ms by a similar process as with NKCOFs. The afforded H_3PO_4@NKCOF-Ms showed high proton conductivity, of which **H_3PO_4@NKCOF-1-M** was the highest at 6.41×10^{-2} S cm^{-1} (Figure S61 and Table S5). After assembling **H_3PO_4@NKCOF-1-M** into an MEA, a maximum power density of 70 mW cm^{-2} (Figure S62) was achieved, slightly lower than that of **H_3PO_4@NKCOF-1** (thin pellet).

Conclusion

In conclusion, we created a stepwise synthesis strategy to prepare COFs with multiple bond linkages resulting in the synthesis of a series of highly robust COFs (NKCOFs) with abundant proton-accepting and donating groups. NKCOFs not only possessed high crystallinity and surface areas, but also displayed outstanding stability in various harsh conditions such as treating with organic solvents, boiling water, and strong acid or base (e.g. 12 M HCl or NaOH). These structural features and outstanding stability endow NKCOFs with high potential for proton conduction application. Indeed, NKCOFs loaded with H_3PO_4 (H_3PO_4@NKCOFs) set a new proton conductivity record (1.13×10^{-1} S cm^{-1} at 80 °C under 98% RH) among all reported COFs. Finally, we successfully fabricated membrane electrode assemblies and applied them in real PEM fuel cells. Notably, **H_3PO_4@NKCOF-1** set a new benchmark for all COF materials, a maximum power density of 81 mW cm^{-2} and a maximum current density of 456 mA cm^{-2}. This work provides important guidance on designing multifunctional COFs, and the synthesis strategy reported in this study is of broad scope, likely applicable to other COF systems. Moreover, this study not only creates new records for superprotonic conductivity, but also achieves presently the best performance of PEM fuel cells for COFs.

Acknowledgements

The authors acknowledge the National Natural Science Foundation of China (21971126) and 111 projects (B12015).

Conflict of interest

The authors declare no conflict of interest.

Keywords: covalent organic frameworks · fuel cells · membranes · multiple-bond linkages · proton conduction

How to cite: *Angew. Chem. Int. Ed.* **2020**, *59*, 3678–3684
Angew. Chem. **2020**, *132*, 3707–3713

[1] N. Armaroli, V. Balzani, *Angew. Chem. Int. Ed.* **2007**, *46*, 52–66; *Angew. Chem.* **2007**, *119*, 52–67.
[2] W. Lubitz, W. Tumas, *Chem. Rev.* **2007**, *107*, 3900–3903.
[3] M. J. Shultz, M. Kelly, L. Paritsky, J. Wagner, *J. Chem. Educ.* **2009**, *86*, 1051–1053.
[4] U. Eberle, M. Felderhoff, F. Schüth, *Angew. Chem. Int. Ed.* **2009**, *48*, 6608–6630; *Angew. Chem.* **2009**, *121*, 6732–6757.
[5] M. Z. Jacobson, W. G. Colella, *Science* **2005**, *308*, 1901–1905.
[6] W. Gao, G. Wu, M. T. Janicke, D. A. Cullen, R. Mukundan, J. K. Baldwin, E. L. Brosha, C. Galande, P. M. Ajayan, K. L. More, A. M. Dattelbaum, P. Zelenay, *Angew. Chem. Int. Ed.* **2014**, *53*, 3588–3593; *Angew. Chem.* **2014**, *126*, 3662–3667.
[7] M. A. Hickner, H. Ghassemi, Y. S. Kim, B. R. Einsla, J. E. McGrath, *Chem. Rev.* **2004**, *104*, 4587–4612.
[8] M. Sadakiyo, T. Yamada, H. Kitagawa, *J. Am. Chem. Soc.* **2009**, *131*, 9906–9907.
[9] P. G. M. Mileo, K. Adil, L. Davis, A. Cadiau, Y. Belmabkhout, H. Aggarwal, G. Maurin, M. Eddaoudi, S. Devautour-Vinot, *J. Am. Chem. Soc.* **2018**, *140*, 13156–13160.
[10] S. Hu, M. Lozada-Hidalgo, F. Wang, A. Mishchenko, F. Schedin, R. R. Nair, E. W. Hill, D. W. Boukhvalov, M. I. Katsnelson, R. A. W. Dryfe, I. V. Grigorieva, H. A. Wu, A. K. Geim, *Nature* **2014**, *516*, 227–230.
[11] L. Mogg, G. Hao, S. Zhang, C. Bacaksiz, Y. Zou, S. J. Haigh, F. M. Peeters, A. K. Geim, M. Lozada-Hidalgo, *Nat. Nanotechnol.* **2019**, *14*, 962–966.
[12] K. A. Mauritz, R. B. Moore, *Chem. Rev.* **2004**, *104*, 4535–4585.
[13] A. Kraytsberg, Y. Ein-Eli, *Energy Fuels* **2014**, *28*, 7303–7330.
[14] H. Zhang, P. Shen, *Chem. Rev.* **2012**, *112*, 2780–2832.
[15] R. F. Service, *Science* **2006**, *312*, 35.
[16] M. Adamski, T. J. G. Skalski, B. Britton, T. J. Peckham, L. Metzler, S. Holdcroft, *Angew. Chem. Int. Ed.* **2017**, *56*, 9058–9061; *Angew. Chem.* **2017**, *129*, 9186–9189.
[17] J. Miyake, R. Taki, T. Mochizuki, R. Shimizu, R. Akiyama, M. Uchida, K. Miyatake, *Sci. Adv.* **2017**, *3*, eaao0476.

[18] Z. Zhou, S. Li, Y. Zhang, M. Liu, W. Li, *J. Am. Chem. Soc.* **2005**, *127*, 18024 – 18025.
[19] N. Asano, M. Aoki, S. Suzuki, K. Miyatake, H. Uchida, M. Watanabe, *J. Am. Chem. Soc.* **2006**, *128*, 1762 – 1769.
[20] J. A. Mader, B. C. Benicewicz, *Macromolecules* **2010**, *43*, 6706 – 6715.
[21] E. B. Trigg, T. W. Gaines, M. Maréchal, D. E. Moed, P. Rannou, K. B. Wagener, M. J. Stevens, K. I. Winey, *Nat. Mater.* **2018**, *17*, 725 – 731.
[22] X. Meng, H. Wang, S. Song, H. Zhang, *Chem. Soc. Rev.* **2017**, *46*, 464 – 480.
[23] A. P. Cote, A. I. Benin, N. W. O'ckwig, M. O'Keeffe, A. J. Matzger, O. M. Yaghi, *Science* **2005**, *310*, 1166 – 1170.
[24] S. Das, P. Heasman, T. Ben, S. Qiu, *Chem. Rev.* **2017**, *117*, 1515 – 1563.
[25] C. S. Diercks, O. M. Yaghi, *Science* **2017**, *355*, eaal1585.
[26] R. P. Bisbey, W. R. Dichtel, *ACS Cent. Sci.* **2017**, *3*, 533 – 543.
[27] M. S. Lohse, T. Bein, *Adv. Funct. Mater.* **2018**, *28*, 1705553.
[28] X. Chen, K. Geng, R. Liu, K. Tan, Y. Gong, Z. Li, S. Tao, Q. Jiang, D. Jiang, *Angew. Chem. Int. Ed.* **2019**, https://doi.org/10.1002/anie.201904291; *Angew. Chem.* **2019**, https://doi.org/10.1002/ange.201904291.
[29] Q. Sun, Y. Tang, B. Aguila, S. Wang, F. Xiao, P. K. Thallapally, A. M. Al-Enizi, A. Nafady, S. Ma, *Angew. Chem. Int. Ed.* **2019**, *58*, 8670 – 8675; *Angew. Chem.* **2019**, *131*, 8762 – 8767.
[30] F. Beuerle, B. Gole, *Angew. Chem. Int. Ed.* **2018**, *57*, 4850 – 4878; *Angew. Chem.* **2018**, *130*, 4942 – 4972.
[31] a) J. Zhang, X. Han, X. Wu, Y. Liu, Y. Cui, *J. Am. Chem. Soc.* **2017**, *139*, 8277 – 8285; b) K. C. Ranjeesh, R. Illathvalappil, V. C. Wakchaure, Goudappagouda, S. Kurungot, S. S. Babu, *ACS Appl. Energy Mater.* **2018**, *1*, 6442 – 6450.
[32] a) L. Wang, J. Zhou, Y. Lan, S. Ding, W. Yu, W. Wang, *Angew. Chem. Int. Ed.* **2019**, *58*, 9443 – 9447; *Angew. Chem.* **2019**, *131*, 9543 – 9547; b) K. C. Ranjeesh, L. George, V. C. Wakchaure, Goudappagouda, R. N. Devi, S. S. Babu, *Chem. Commun.* **2019**, *55*, 1627 – 1630.
[33] S. Jiang, S. Gan, X. Zhang, H. Li, Q. Qi, F. Cui, J. Lu, X. Zhao, *J. Am. Chem. Soc.* **2019**, *141*, 14981 – 14986.
[34] a) Y. Hu, N. Dunlap, S. Wan, S. Lu, S. Huang, I. Sellinger, M. Ortiz, Y. Jin, S. Lee, W. Zhang, *J. Am. Chem. Soc.* **2019**, *141*, 7518 – 7525; b) E. Vitaku, W. R. Dichtel, *J. Am. Chem. Soc.* **2017**, *139*, 12911 – 12914.
[35] D. A. Pyles, W. H. Coldren, G. M. Eder, C. M. Hadad, P. L. McGrier, *Chem. Sci.* **2018**, *9*, 6417 – 6423.
[36] M. Matsumoto, L. Valentino, G. M. Stiehl, H. B. Balch, A. R. Corcos, F. Wang, D. C. Ralph, B. J. Marin, W. R. Dichtel, *Chem* **2018**, *4*, 308 – 317.
[37] a) K. Dey, M. Pal, K. Rout, S. H. Kunjattu, A. Das, R. Mukherjee, U. K. Kharul, R. Banerjee, *J. Am. Chem. Soc.* **2017**, *139*, 13083 – 13091; b) A. Halder, M. Ghosh, M. A. Khayum, S. Bera, M. Addicoat, H. S. Sasmal, S. Karak, S. Kurungot, R. Banerjee, *J. Am. Chem. Soc.* **2018**, *140*, 10941 – 10945.
[38] Z. Wang, Q. Yu, Y. Huang, H. An, Y. Zhao, Y. Feng, X. Li, X. Shi, J. Liang, F. Pan, P. Cheng, Y. Chen, S. Ma, Z. Zhang, *ACS Cent. Sci.* **2019**, *5*, 1352 – 1359.
[39] a) P. Shao, J. Li, F. Chen, L. Ma, Q. Li, M. Zhang, J. Zhou, A. Yin, X. Feng, B. Wang, *Angew. Chem. Int. Ed.* **2018**, *57*, 16501 – 16505; *Angew. Chem.* **2018**, *130*, 16739 – 16743; b) H. Wang, Z. Zeng, P. Xu, L. Li, G. Zeng, R. Xiao, Z. Tang, D. Huang, L. Tang, C. Lai, D. Jiang, Y. Liu, H. Yi, L. Qin, S. Ye, X. Rena, W. Tang, *Chem. Soc. Rev.* **2019**, *48*, 488 – 516; c) C. Zhang, B. Wu, M. Ma, Z. Wang, Z. Xu, *Chem. Soc. Rev.* **2019**, *48*, 3811 – 3841.
[40] H. S. Sasmal, H. B. Aiyappa, S. N. Bhange, S. Karak, A. Halder, S. Kurungot, R. Banerjee, *Angew. Chem. Int. Ed.* **2018**, *57*, 10894 – 10898; *Angew. Chem.* **2018**, *130*, 11060 – 11064.
[41] a) Y. Peng, G. Xu, Z. Hu, Y. Cheng, C. Chi, D. Yuan, H. Cheng, D. Zhao, *ACS Appl. Mater. Interfaces* **2016**, *8*, 18505 – 18512; b) K. Ranjeesh, R. Illathvalappil, S. Veer, J. Peter, V. Wakchaure, Goudappagouda, V. Raj, S. Kurungot, S. S. Babu, *J. Am. Chem. Soc.* **2019**, *141*, 14950 – 14954.
[42] S. Chandra, T. Kundu, S. Kandambeth, R. BabaRao, Y. Marathe, S. M. Kunjir, R. Banerjee, *J. Am. Chem. Soc.* **2014**, *136*, 6570 – 6573.
[43] H. Ma, B. Liu, B. Li, L. Zhang, Y. Li, H. Tan, H. Zang, G. Zhu, *J. Am. Chem. Soc.* **2016**, *138*, 5897 – 5903.
[44] C. Montoro, D. Rodríguez-San-Miguel, E. Polo, R. Escudero-Cid, M. Ruiz-Gonzalez, J. A. R. Navarro, P. Ocon, F. Zamora, *J. Am. Chem. Soc.* **2017**, *139*, 10079 – 10086.
[45] M. Zheng, A. Aylin, M. A. Katherine, *Chem. Mater.* **2019**, *31*, 819 – 825.
[46] H. Xu, S. Tao, D. Jiang, *Nat. Mater.* **2016**, *15*, 722 – 727.
[47] a) L. Halasz, K. Lukic, H. Vancik, *Acta Crystallogr. Sect. C* **2007**, *63*, o61 – o64; b) A. M. Sanchez, M. Barra, R. H. de Rossi, *J. Org. Chem.* **1999**, *64*, 1604 – 1609.
[48] Z. Zhang, H. Nguyen, S. A. Miller, S. M. Cohen, *Angew. Chem. Int. Ed.* **2015**, *54*, 6152 – 6157; *Angew. Chem.* **2015**, *127*, 6250 – 6255.
[49] P. Ramaswamy, N. E. Wong, G. K. H. Shimizu, *Chem. Soc. Rev.* **2014**, *43*, 5913 – 5932.
[50] G. Xing, T. Yan, S. Das, T. Ben, S. Qiu, *Angew. Chem. Int. Ed.* **2018**, *57*, 5345 – 5349; *Angew. Chem.* **2018**, *131*, 5443 – 5447.
[51] S. Kandambeth, A. Mallick, B. Lukose, M. V. Mane, T. Heine, R. Banerjee, *J. Am. Chem. Soc.* **2012**, *134*, 19524 – 19527.
[52] L. Vilčiauskas, M. E. Tuckerman, G. Bester, S. J. Paddison, K. D. Kreuer, *Nat. Chem.* **2012**, *4*, 461 – 466.
[53] W. Kong, W. Jia, R. Wang, Y. Gong, C. Wang, P. Wu, J. Guo, *Chem. Commun.* **2019**, *55*, 75 – 78.
[54] X. Wu, X. Wang, G. He, J. Benziger, *J. Polym. Sci. Part B* **2011**, *49*, 1437 – 1445.

Manuscript received: October 29, 2019
Revised manuscript received: December 12, 2019
Accepted manuscript online: December 13, 2019
Version of record online: January 20, 2020

